20th Australasian Fluid Mechanics Conference
Perth, Australia
5-8 December 2016

Numerical Investigation of Diesel Exhaust Particle Transport and Deposition in up to 17 Generations of the Lung Airway

Mohammad S. Islam[1], Suvash C. Saha[1], Emilie Sauret[1], and Y.T. Gu[1]
[1]*School of Chemistry, Physics & Mechanical Engineering, Queensland University of Technology*
2 George Street, GPO Box 2434, Brisbane QLD 4001, Australia

Abstract

Diesel exhaust particulates matter (DEPM) is a compound mixture of gases and fine particles that contains more than 40 toxic air pollutants including benzene, formaldehyde, and nitrogen oxides. Exposure of DEPM to human lung airway during respiratory inhalation causes severe health hazards like diverse pulmonary diseases. This paper studies the DEPM transport and deposition in upper 17-generation of digital lung airways. The Euler-Lagrange approach is used to solve the continuum and disperse phases of the calculation. Lagrangian based Discrete Phase Model (DPM) is used to investigate the DEPM nanoparticle dispersion and deposition in the current anatomical model. The effects of size specific monodispersed particles on deposition are extensively investigated during resting condition. The numerical results illustrate that Brownian diffusion is the dominant mechanism for smaller diameter particles. The present 17-generation bifurcation model also depicts different deposition hot spot for various diameter particles which could advance the understanding of the therapeutic drug delivery system to the specific position of the respiratory airways.

Introduction

DEPM is a compound that contains different types of toxic and non-toxic substances. Polycyclic aromatic hydrocarbons (PAHs), nitro-PAHs, carbon monoxide, sulphur, nitrogen compounds and several low molecular weight hydrocarbons are the main element of DEPM. Among all of the pollutant particulates in the atmosphere, DEPM is the most pernicious for human health due to its physical properties and toxicity. Exposure of DEPM to the human lung during respiratory inhalation causes severe health hazards like diverse pulmonary diseases [1]. For example, the acute health risks of DEPM inhalation can cause lung cancer. In the current century, diesel engine furnished automobiles, and light-duty transport have significantly increased. Diesel engine based automobiles are getting much popular due to its greater energy efficiency than other engines. Despite its higher energy competency, diesel engine produces and discharge higher pollutant substance than other engines [2].

The diesel exhaust particles size is generally less than 1 μm. Realistically, DEPM can be sub-micro and micro size. In the accumulation mode of a diesel engine, DEPM aerodynamic diameter is 0.03-0.5 μm, and the diesel exhaust particles can be 1-10 μm in coarse mode [3]. DEPM can enter at the deeper airways depending on its size distribution and breathing pattern variation. At the resting condition, inlet flow rate is very low (9 lpm) and ultrafine particle (d<100nm) can easily enter into the alveoli. The available *in silico* model has improved the understanding of the nanoparticle deposition in the upper airways, but the adequate nanoparticle transport and deposition data in the deeper airways is still unknown. Cohen et al. [4] have investigated the ultrafine particle deposition pattern at the tracheobronchial region of the human lung. Zhang et al. [5] have investigated the micro- and nano-particle deposition pattern at the upper airways for 15 lpm flow rate. There have been a few studies incorporating the nanoparticle deposition in the upper airways [6, 7]. Recently, Islam et al. [8] have investigated the aerosol particle transport and deposition in the realistic lung airway of the human lung. Their CT-based anatomical model showed a new deposition pattern for the central airway. No computational or experimental study has been conducted for the nanoparticle transport and deposition in the 17-generation of the human lung at resting condition.

In the present study, DEPM nanoparticle transport and deposition for the 17-generation anatomical model is investigated for resting condition. This study also illustrates the influence of DEPM aerodynamic size distribution of respiratory deposition.

Methods

The 17-generation anatomical model employed in the present study is the best published explicit lung airway model proposed by Schmidt et al. [9]. The digital airway geometry contains 1453 bronchi, including the central and lower tracheobronchial airways [10]. The unstructured tetrahedral mesh and a fine boundary layer inflation mesh with a ten layer dense hexahedral element was generated near the wall to simulate the complex flow behavior. The transition ratio value 0.272 was used to create the inflation layer near the wall. A dense tetrahedral element was used at bifurcation area of the geometry. A proper grid refinement test has been performed and final geometry contains about 34 million cells. Lagrangian particle tracking scheme is used to investigate the particle transport and deposition in the 17-generation airway. ANSYS 17.0 (FLUENT) solver based Discrete Phase Model (DPM) is used to monitor the DEPM impact on the lung surface. The mass (1) and the momentum equations (2) were solved to calculate the air flow.

$$\frac{\partial \rho}{\partial t} + \nabla \cdot (\rho \vec{v}) = S_m \tag{1}$$

where S_m is the mass source term.

$$\frac{\partial}{\partial t}(\rho \vec{v}) + \nabla \cdot (\rho \vec{v}\vec{v}) = -\nabla p + \nabla \cdot \left(\mu \left[\left(\nabla \vec{v} + \nabla \vec{v}^T \right) - \frac{2}{3} \nabla \cdot \vec{v} I \right] \right) + \rho \vec{g} + \vec{F} \tag{2}$$

where, p is fluid static pressure, $\rho \vec{g}$ is body force due to gravity, and $\vec{F}$ is body force due to external (particle-fluid interaction) force. Pressure-velocity coupling scheme, SIMPLE is used to solve the DPM particle movement. A parabolic inlet condition for laminar flow [11] is used,

$$u(r) = 2u_{av}\left(1 - \frac{r^2}{R^2}\right) \tag{3}$$

where R is the pipe radius.

To model the nano-particles, Brownian motion is considered. Appropriate particle motion equation [12] is solved to calculate the individual particles.

$$\frac{du_i^p}{dt} = F_D(u_i^g - u_i^p) + F_{Brownian} + F_{Lift} + \frac{\rho_p - \rho_g}{\rho_p} g_i$$

$$F_D = \frac{18\mu_g}{\rho_p d_p^2 C_c} \qquad (4)$$

$$C_c = 1 + \frac{2\lambda}{d_p}(1.257 + 0.4e^{-1.1 d_p / 2\lambda})$$

Where F_D is the drag force per unit particle mass, Re_p is the particle Reynolds number, and C_c is the Cunningham correction factor. The specific Cunningham correction factor is employed for different diameter particles. The density of the particle is used as $1100\, kg/m^3$. Tracking parameter length scale 0.000005 is used for the present model. The velocity inlet and zero pressure outlet boundary condition are used to address the equation of flow. The wall boundary condition is set as a trap to investigate the particle impact on the wall.

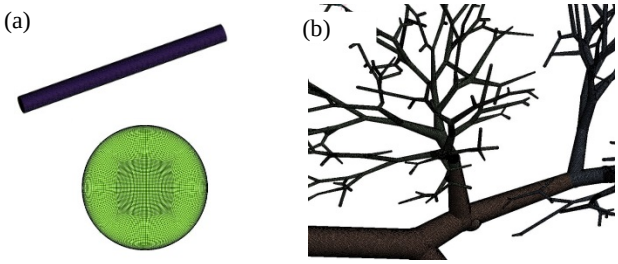

Figure 1.(a) Straight pipe geometry and generated mesh, and (b) mesh in the 17-generation geometry.

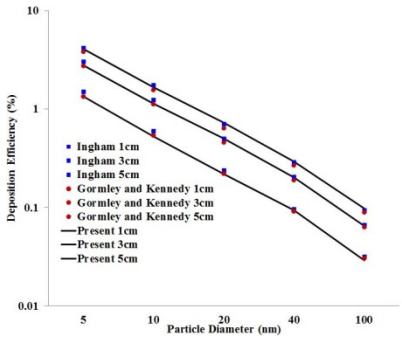

Figure 2. Deposition efficiency comparison at 1m/s inlet velocity in 4.5 mm diameter straight pipe with different pipe length.

To validate the present model, a straight pipe is constructed. Figure 1(a) shows the straight pipe geometry and the inlet mesh of the pipe. Figure 1(b) shows the mesh of the 17-generation geometry. Deposition efficiency of different diameter particles is validated with the published results [13, 14] for 4.5 mm diameter straight pipe and 1m/s inlet velocity. Figure 2 shows the deposition efficiency comparison and the present result shows a good agreement with the published result.

Results and Discussions

The present study accounts for nanoparticle transport and deposition in up to 17 generations of a digital airway geometry. The current study comprehensively investigated the nanoparticle transport and deposition pattern at resting condition. According to the ICRP, the flow rates 9 lpm is considered as rest-activity [15]. 1-nm, 10-nm, 50-nm, and 1000-nm diameter particles are considered in the present study.

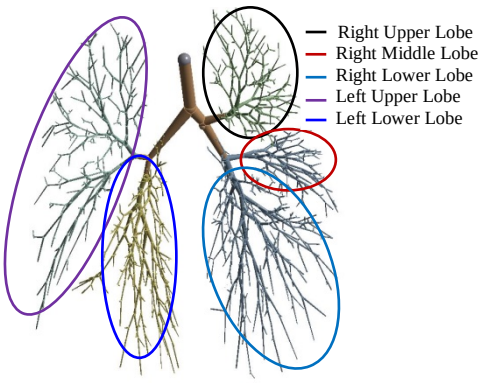

Figure 3. Schematic diagrams of the different lobes of the 17-generation anatomical model.

Figure 3 shows different lobes of the 17-generation airway model. The right lung consists three lobes, while the left lung contains two lobes.

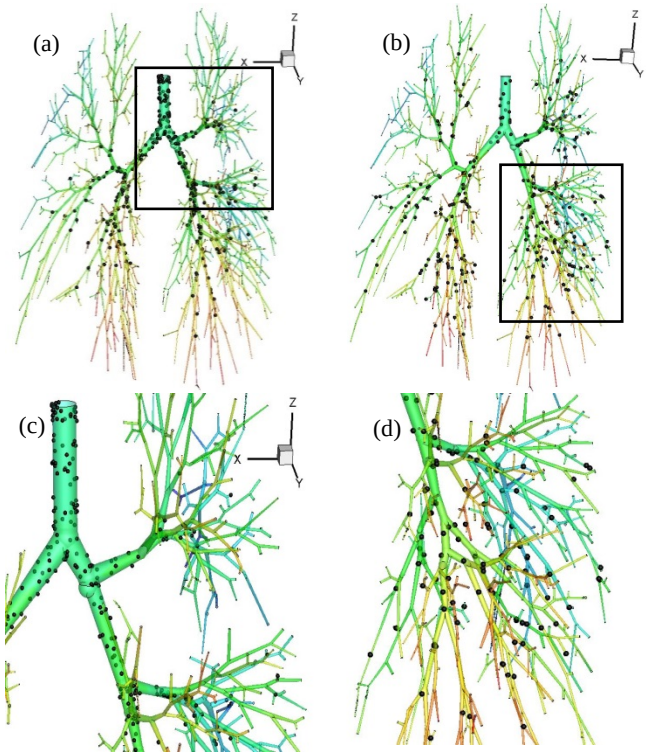

Figure 4. Monodisperse particle deposition pattern at 9 lpm flow rate for (a) 1-nm particle, (b) 10-nm particle, (c) enlarged portion of figure 4(a), and (d) enlarged portion of figure 4(b).

Figure 4 (a, b) show 1-nm, and 10-nm diameter particle deposition pattern respectively at 9 lpm flow rate. The deposition pattern shows large numbers of particles are deposited at the very top of the trachea and first couple of generations for 1-nm diameter particle. On the contrary, for 10-nm diameter particle, less number of particles are deposited at the trachea. Figure 4(c, d) show the enlarged portion of figure 4(a, b) respectively. The deposition pattern shows diffusion is dominant in the first couple of generation for the 1-nm particle. Brownian motion is the random microscopic motion of the smaller particles due to the frequent chaotic collision by gas molecules. Gas molecules collision mainly causes the diffusion, and that is why the Brownian motion effectiveness increases with the decrease of particle diameter. The 1-nm diameter particle deposition pattern shows a similar deposition pattern for Brownian motion

simulation. Figure 4(d) shows the deposition pattern at the deeper airways. Due to the smaller size of the particle, 1-nm and 10-nm diameter particles can easily enter into the deeper airways. Therefore, a large number of 1-nm and 10-nm diameter particles are deposited at the 17-generation of the digital airway model. A significant amount of 1-nm and 10-nm diameter particles are escaped through the outlets of the 17-generation, and the escaped particle would eventually enter into the 18th generation of the lung airway. The escaped particle will travel up to 23rd generations of the lung, and some of the particles will deposit into the rest of the generations. Some particle could enter into the alveoli, and they might be absorbed into the bloodstream of the human body by crossing the alveolar epithelial wall.

Figure 5(a, b, c) show the deposition pattern for 7.5 lpm, 9 lpm, and 25 lpm flow rate respectively for 50-nm diameter particle. Figure 5(d) show the deposition density comparison for three different flow rates. The deposition pattern illustrates that less number of particles are deposited at the trachea, and a noticeable amount of particles are deposited at the carinal angle of the upper airways. The deposition concentration depicts that Brownian motion effectiveness decreases with the increases in particle diameter at the trachea. Figure 5(a, b, c) show enormous amounts of 50-nm diameter particle are deposited at the bifurcation angle and the bifurcation branches of the both lungs regardless of the flow rates. The effectiveness of the diffusion decreases with the increases in the particle diameter due to the higher inertia of the larger particle. Due to the larger inertia, inertial impaction is dominant in the bifurcation angles, and that is the reason a large number of particle is deposited at the tracheobronchial airways.

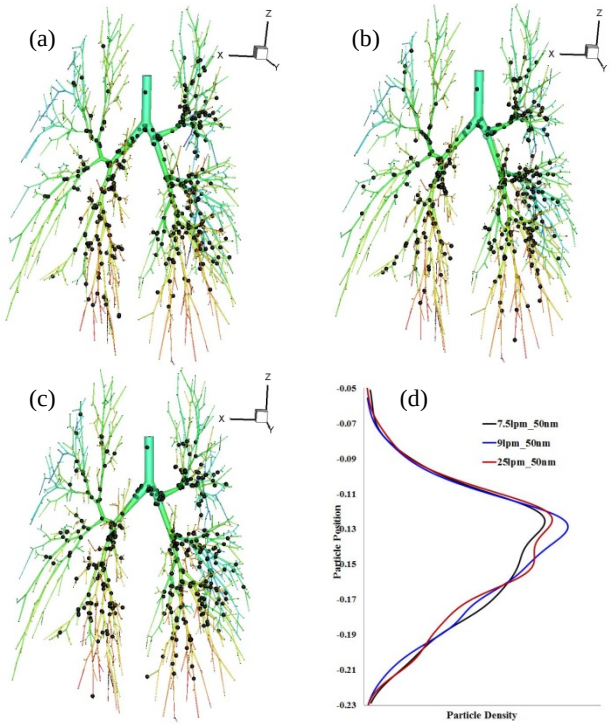

Figure 5. Monodisperse particle deposition pattern for 50 nm diameter particles at, (a) 7.5 lpm, (b) 9 lpm, and (c) 25 lpm flow rates, and (d) deposition density comparison.

Figure 6(a) shows the 1000-nm diameter particle deposition pattern at 9 lpm flow rate. Figure 6(b) presents the enlarged portion of figure 6(a). The deposition scenario depicts that no particles are deposited at the trachea, and the deposition concentration is mostly high at the bifurcation area. The present anatomical model asymmetricity and the larger particle inertia are the main reason for this type of deposition. The current digital airway model is highly asymmetric, and the surface of the bifurcation branches consist uneven bends and waves. The larger particle (micro-particle) has large inertia, and particle follows the air streamline. At higher flow rate, the larger particle cannot follow the air streamline when the particle faces any obstacle due to higher inertia. As a result, it deviates from the streamline and gets contact with the lung wall. That is why; 1000-nm diameter particle shows the deposition concentration is mostly high at the bifurcation area.

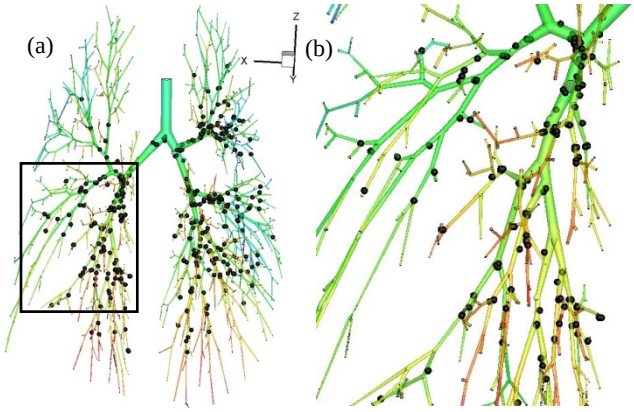

Figure 6(a) Monodisperse particle deposition pattern at 9 lpm flow rate for 1000nm diameter particle, and (b) the enlarged portion of figure 5(a).

Figure 7 shows the deposition density comparison at the right and the left lung of the 17-generation airway model for different diameter particle. The density curve clearly shows, for 1-nm particle deposition concentration at the upper airways of the both lungs are higher than other size particle. The deposition density at right lung is higher than the left lung for 1-nm diameter particle. The deposition density curve also illustrates that the deposition concentration at the right lung is higher than the left lung at the upper airways. On the contrary, the deposition concentration of the left lung is higher than the right lung in the conducting airways. The asymmetric anatomical model of the right and the left lung, and the deposition mechanisms are the main reason for the deposition density difference at the right and the left lung.

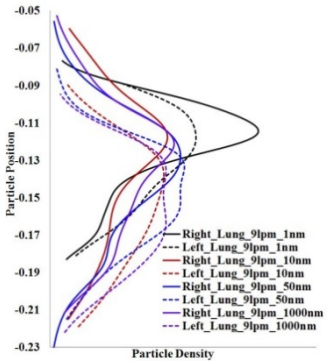

Figure 7. The deposition density comparison at right lung and the left lung of the 17-generation digital airway for different diameter particle.

Figure 8 shows the deposition density comparison at the five different lobes of the right and the left lung for different diameter particles. The overall deposition illustrates that the deposition efficiency at different lobes is different based on different size particle. Figure 8 depicts that the deposition efficiency at the right lower lobe is higher than the other lobes no matter whatever the particles diameter are. The deposition efficiency of 1-nm diameter particle is higher in the right lower lobe and the left lower lobe than the other lobes, which also describes that smaller size particle can reach the alveolar region.

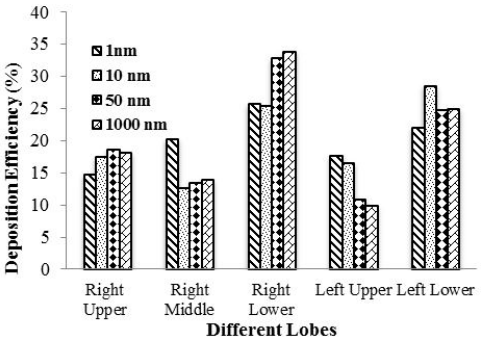

Figure 8. Deposition efficiency comparison at different lobes of the right and left lung for different size particle (deposition efficiency at various lobes are calculated based on the number of deposited particles for different size particles).

Figure 9 shows the deposition efficiency and percentage of the escaped particle at 9 lpm flow rate. The deposition efficiency increases with the increase of particle diameter. Figure 9 shows a significant amount of particles are escaped through the outlets of the 17-genration model. These escaped particle might be deposited in the alveolar region. Depending on the residence time and toxicity of the deposited particle in the lung airways and bloodstream, the particle can occur severe health hazards.

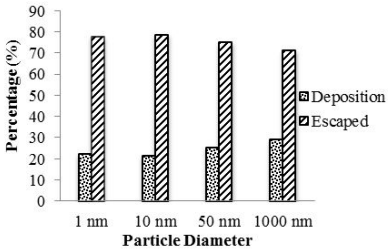

Figure 9. Deposition efficiency and percentage of escaped particle comparison.

Conclusions

The present numerical model illustrates the monodisperse nanoparticle transport and deposition in the upper 17-generation of the human lung. A numerical model is developed to predict the nanoparticle transport and deposition in the digital airway geometry. The first ever 17-generation nano-particle investigation addressed the lack of the nanoparticle transport and deposition in the deeper airways. The following conclusions can be drawn from the present study:

- Brownian diffusion is dominant for 1-nm diameter particle deposition, and the lung wall surface is the deposition hot spot. Brownian motion effectiveness decreases with the increase of particle diameter;
- Deposition efficiency at different lobes is unlike for various diameter particle;
- A higher number of particles are deposited in the right lung compare to left lung.

The findings of the present study and more inclusive size specific polydisperse particle investigation will help the understanding of the drug delivery system to the alveolar region. The present model can identify the zone specific deposition hot spot, which could potentially assist the health risk assessment system. A more comprehensive polydisperse nanoparticle transport and deposition for the digital airway geometry will be studied in the near future.

Acknowledgment

The authors thankfully acknowledge Dr. Tevfik Gemci for providing the 17-generation geometry of the human lung. The authors also would like to thank the high-performance computing (HPC) Unit, Queensland University of Technology, Australia.

References

1. McClellan, R. O., *Health effects of exposure to diesel exhaust particles.* Annual review of pharmacology and toxicology, 1987. **27**(1): p. 279-300.
2. Cuddihy, R. G., Griffith, W., Clark, C., and McClellan, R., *Potential health and environmental effects of light duty diesel vehicles. II.* 1981, Lovelace Biomedical and Environmental Research Inst., Albuquerque, NM (USA). Inhalation Toxicology Research Inst.
3. Abdul-Khalek, I., Kittelson, D., and Brear, F., *The influence of dilution conditions on diesel exhaust particle size distribution measurements*. 1999, SAE Technical paper.
4. Cohen, B. S., Sussman, R. G., and Lippmann, M., *Ultrafine particle deposition in a human tracheobronchial cast.* Aerosol Science and Technology, 1990. **12**(4): p. 1082-1091.
5. Zhang, Z., Kleinstreuer, C., Donohue, J. F., and Kim, C. S., *Comparison of micro- and nano-size particle depositions in a human upper airway model.* Journal of Aerosol Science, 2005. **36**(2): p. 211-233.
6. Farhadi Ghalati, P., Keshavarzian, E., Abouali, O., Faramarzi, A., Tu, J., and Shakibafard, A., *Numerical analysis of micro- and nano-particle deposition in a realistic human upper airway.* Computers in Biology and Medicine, 2012. **42**(1): p. 39-49.
7. Zhang, Z., Kleinstreuer, C., Donohue, J., and Kim, C., *Comparison of micro-and nano-size particle depositions in a human upper airway model.* Journal of aerosol science, 2005. **36**(2): p. 211-233.
8. Islam, M. S., Saha, S. C., Sauret, E., Gu, Y., and Ristovski, Z. *Numerical investigation of aerosol particle transport and deposition in realistic lung airway*. in *Proceedings of the International Conference on Computational Methods*. 2015. Scientech Publisher llc, USA.
9. Schmidt, A., Zidowitz, S., Kriete, A., Denhard, T., Krass, S., and Peitgen, H.-O., *A digital reference model of the human bronchial tree.* Computerized Medical Imaging and Graphics, 2004. **28**(4): p. 203-211.
10. Gemci, T., Ponyavin, V., Chen, Y., Chen, H., and Collins, R., *Computational model of airflow in upper 17 generations of human respiratory tract.* Journal of Biomechanics, 2008. **41**(9): p. 2047-2054.
11. White, F. M., *Fluid mechanics. 5th.* Boston: McGraw-Hill Book Company, 2003.
12. Inthavong, K., Tu, J., and Ahmadi, G., *Computational modelling of gas-particle flows with different particle morphology in the human nasal cavity.* The Journal of Computational Multiphase Flows, 2009. **1**(1): p. 57-82.
13. Gormley, P. and Kennedy, M. *Diffusion from a stream flowing through a cylindrical tube.* in *Proceedings of the Royal Irish Academy. Section A: Mathematical and Physical Sciences*. 1948. JSTOR.
14. Ingham, D., *Diffusion of aerosols from a stream flowing through a cylindrical tube.* Journal of Aerosol Science, 1975. **6**(2): p. 125-132.
15. ICRP and Protection, I. C. o. R., *ICRP Publication 66: Human Respiratory Tract Model for Radiological Protection*. 1994: Elsevier Health Sciences.